A&A, 711, A272 (2026)
https://doi.org/10.1051/0004-6361/202660397

Astronomy & Astrophysics

High-resolution laboratory study of the ν_2/ν_4 bending motion of CH_3^+ and assignment of its astronomically observed lines

Thomas Salomon[1,⋆], Ilane Schroetter[2], Olivier Berné[2], P. Bryan Changala[3,4], Marie-Aline Martin-Drumel[5], Yoko Okada[1], Markus Röllig[6,7,1], Stephan Schlemmer[1], and Oskar Asvany[1]

[1] I. Physikalisches Institut, Universität zu Köln, Zülpicher Str. 77, 50937 Köln, Germany
[2] Institut de Recherche en Astrophysique et Planétologie, Université de Toulouse, CNRS, CNES, UPS, 9 Av. du colonel Roche, 31028 Toulouse Cedex 04, France
[3] JILA, University of Colorado Boulder & National Institute of Standards and Technology, Boulder, CO 80309, USA
[4] Department of Physics, University of Colorado Boulder, Boulder, CO 80309, USA
[5] Université Paris-Saclay, CNRS, Institut des Sciences Moléculaires d'Orsay, 91405 Orsay, France
[6] Physikalischer Verein – Gesellschaft für Bildung und Wissenschaft, Robert-Mayer-Straße 2, 60325 Frankfurt am Main, Germany
[7] Institut für Angewandte Physik, Goethe-Universität Frankfurt, Max-von-Laue-Str. 1, 60438 Frankfurt am Main, Germany

Received 13 April 2026 / Accepted 17 June 2026

ABSTRACT

Context. The methyl cation (CH_3^+) was discovered through the detection of a 7 μm (1400 cm^{-1}) band observed in the d203-506 protoplanetary disk in the Orion nebula using the MIRI-MRS spectrometer on board the JWST. This feature has now been reported in numerous astronomical sources. The initial detection was based on simulations of its coinciding and interacting bending modes (ν_2/ν_4) using coarse laboratory and theoretical data, and combined to astronomical data with an absolute wavelength calibration of only several cm^{-1}. A first spectroscopic assignment of the lines was enabled by later quantum chemical calculations. However, a full spectroscopic assignment of the astronomically observed features in the 7 μm range is awaiting high-resolution laboratory measurements and a more robust wavelength calibration of the MIRI-MRS data.
Aims. We present a laboratory high-resolution study of the ν_2/ν_4 bending vibrations of CH_3^+ in order to provide accurate and calibrated data for the spectroscopic analysis of JWST detections of this species.
Methods. The rovibrational structure of the ν_2/ν_4 bending vibrations of CH_3^+ was studied in a cryogenic 22-pole ion trap apparatus at 10 K. For the detection of the vibrational excitation, the efficient leak-out spectroscopy method was used, in combination with a high-resolution quantum cascade laser operating at 7 μm. This was combined with MIRI-MRS data of d203-506 reduced with improved wavelength calibration.
Results. We were able to measure 49 rovibrational lines of the ν_2/ν_4 band up to $J'' = 6$ between 1330 and 1440 cm^{-1} (6.9–7.5 μm) in high resolution. The measurement accuracy and precision of about 0.001 and 0.0007 cm^{-1}, respectively, allow spectroscopic constants and line predictions to be derived with high confidence, and thus permit accurate (Doppler velocity) diagnostics of CH_3^+ lines with JWST.

Key words. astrochemistry – line: identification – molecular data – ISM: abundances – ISM: molecules – photon-dominated region (PDR)

1. Introduction

The methyl cation, CH_3^+, has been long suspected to be an important astrochemical intermediate in the interstellar and circumstellar medium (e.g., Herbst & Klemperer 1973). Due to its planar and triangular geometry, it lacks a permanent dipole moment and cannot be observed by radio astronomy, but only by its vibrational fingerprints in the infrared (IR). Still, it came somewhat as a surprise when Berné et al. (2023) achieved the first conclusive detection of CH_3^+ using the *James Webb* Space Telescope (JWST), toward the UV-irradiated protoplanetary disk d203-506 in the Orion bar. Interestingly, this detection has not been achieved via its C–H stretching vibration ν_3 at 3 μm, well characterized in the laboratory by Crofton et al. (1985, 1988) and Jagod et al. (1994), but at wavelengths around 7 μm (~1400 cm^{-1}) using the Mid-InfraRed Instrument (MIRI) on board JWST. At this wavelength, two bending modes of the cation accidentally coincide and interact, the out-of-plane (ν_2) and degenerate in-plane (ν_4) bending modes, for which high-resolution IR data had been missing at the time of the detection. Since this first detection, follow-up observations of CH_3^+ have been made in many diverse environments at 7 μm (Henning et al. 2024; Zannese et al. 2025; Bhatt et al. 2025; Romero-Mirza et al. 2025; Rocha et al. 2025), which demonstrate that CH_3^+ is indeed ubiquitous in UV-irradiated environments.

Due to missing high-resolution laboratory IR data, the initial detection had to rely on several pieces of spectroscopic evidence: (i) the spectroscopic features around 1400 cm^{-1} were exactly where previous laboratory experiments located the ν_2/ν_4 dyad (Cunha de Miranda et al. 2010; Asvany et al. 2018), and (ii) the resolved rovibrational structure and its spectral span was compatible with a light molecular carrier. More specifically, (iii) a spectroscopic simulation using known experimental data (Crofton et al. 1985, 1988) as well as theoretical studies (Kraemer & Špirko 1991; Yu & Sears 2002; Dopfer & Luckhaus 2002; Keçeli et al. 2009; Thomas et al. 2012; Ragni et al. 2016; Nyman & Yu 2019; Meisner et al. 2019) was able to reproduce

⋆ Corresponding author: salomon@ph1.uni-koeln.de

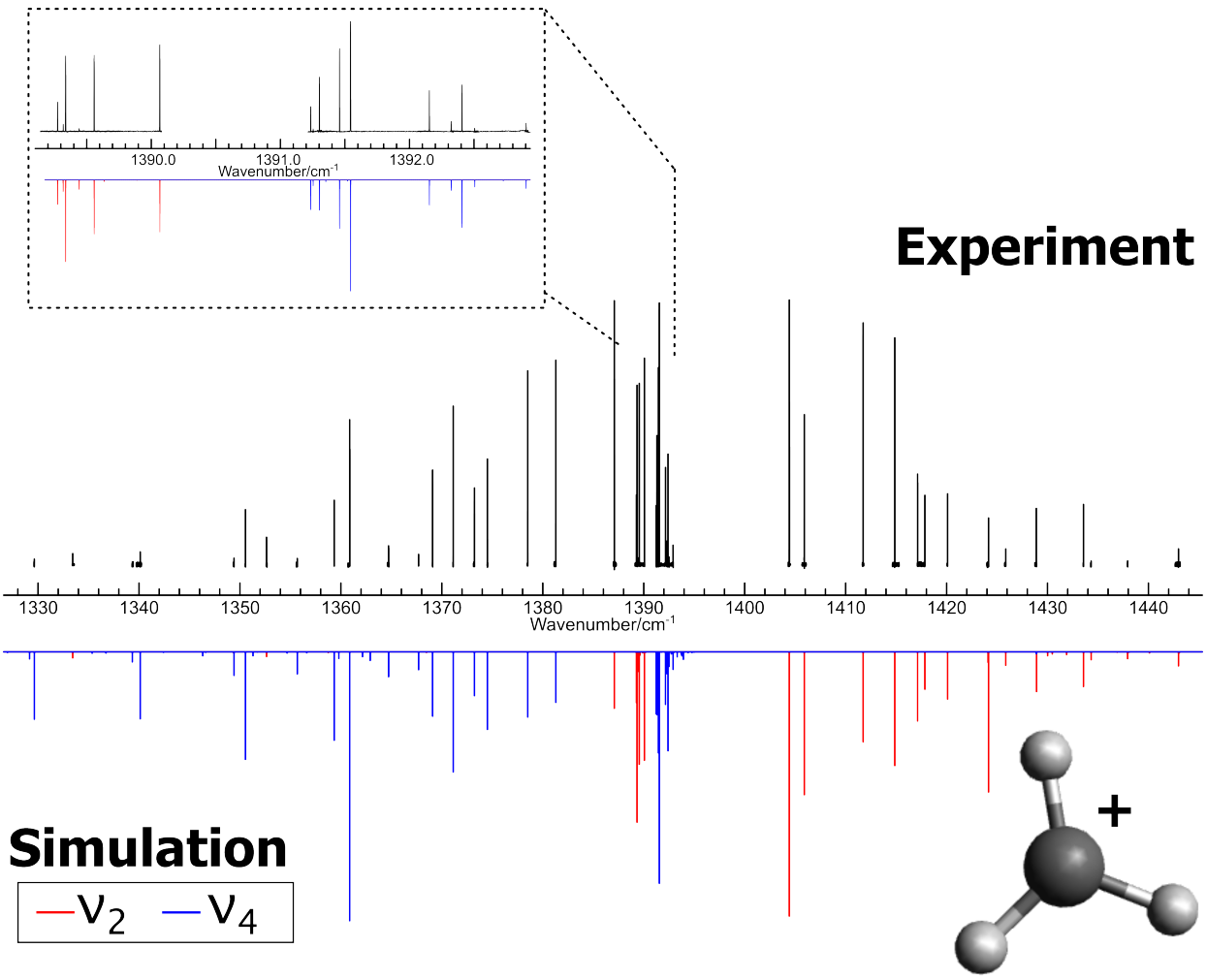

Fig. 1. *Top*: experimental LOS spectrum of the ν_2/ν_4 bending vibrations of CH_3^+. *Bottom*: comparison with a spectroscopic simulation performed at a temperature of 80 K. The two bands are marked in red and blue according to their main contribution. See text for more details. The experimental LOS spectrum is available as supplementary material.

the appearance of the detected JWST observation convincingly, albeit without giving any confident quantum state assignments. Only more recently, in an impressive demonstration of high-level quantum chemical computations, Changala et al. (2023) performed nuclear motion computations on an accurate CCSD(T) potential energy surface of tetra-atomic CH_3^+, by which its spectroscopic parameters could be obtained, in particular the Coriolis coupling constants. A simulation based on these calculations enabled the first spectroscopic assignments, from which the rotational temperature of CH_3^+ in d203-506 could be derived, and its beam-averaged column density estimated. The obtained spectroscopic constants were validated by experimental measurements both of the ν_2/ν_4 dyad of bare CH_3^+ at vibrational resolution, and of the rotationally resolved photoionization spectrum of CH_3 in $v_2 = 1$. Yet, direct high-resolution measurements of the ν_2/ν_4 dyad were missing.

In this work, we finally present the first direct high-resolution measurement and analysis of the ν_2/ν_4 dyad in the 1400 cm^{-1} region of the IR spectrum. This is made possible by the use of the leak-out action spectroscopic method (Schmid et al. 2022) and the recent procurement of a high-resolution IR laser source operating at 7 µm. The analysis is complicated by the strong Coriolis interaction between the accidentally degenerate bending vibrations ν_2 and ν_4, the interaction being more severe than for the similar systems BH_3 and SiH_3^+ (Kawaguchi 1994; Davies & Smith 1994). This is apparently one of the reasons why a previous investigation reported no complete analysis of this dyad (thesis of Joo 1996). The results of this work now allow for the rovibrational lines of the ν_2/ν_4 dyad to be predicted with an accuracy of about 0.001 cm^{-1}, and thus put the JWST detections on a solid laboratory calibration basis.

2. Methodology

The Coriolis-coupled ν_2/ν_4 bending vibrations of CH_3^+ were studied in one of Cologne's cryogenic ion trapping machines, called COLTRAP II (Bast et al. 2023). In brief, CH_3^+ ions were generated in a storage ion source by electron impact ionization of methane, CH_4. Every second, a pulse of several tens of thousands of ions was extracted from the source, selected in a quadrupole mass spectrometer for a mass-to-charge ratio of m/z=15 (CH_3^+), and then injected into the 22-pole trap (Asvany et al. 2010) mounted on a 10 K coldhead. The trap was constantly filled with a 1:3 buffer gas mixture of neon diluted in helium ($\sim 4 \times 10^{13}$ cm^{-3}). Helium functions not only as a collisional partner facilitating the effective trapping and thermalization of incoming cations, but it also plays a crucial role in preventing

significant neon freeze-out on the surfaces of the trap. High-resolution ro-vibrational spectra of confined ions were obtained utilizing the leak-out action spectroscopy method (LOS, Schmid et al. 2022). This technique has proven to be quite universal and practical, with numerous recent applications to astrophysically relevant cations (Schmid et al. 2022; Asvany et al. 2023; Bast et al. 2023; Schlemmer et al. 2024; Silva et al. 2023; Changala et al. 2023; Silva et al. 2024b; Gupta et al. 2023; Steenbakkers et al. 2024; Silva et al. 2024a; Salomon et al. 2025; Gupta et al. 2025). In brief, LOS exploits the fact that the vibrational energy of a laser-excited ion can be converted into kinetic energy in a collision with a suitable neutral molecule or atom. Trial measurements comparing the LOS efficiency of pure helium buffer gas with that of the initially mentioned helium-neon buffer gas mixture were performed. In this study, a helium-neon mixture is employed due to the more advantageous mass ratio between CH_3^+ ions and neon in comparison to that with helium. CH_3^+ ions undergoing the vibration-to-translation energy transfer may escape the ion trap and are steered toward a Daly-type ion detector. By repeating these cycles at 1 Hz and counting the "leaked-out" CH_3^+ ions as a function of the laser wavenumber, a rovibrational spectrum is obtained.

The IR excitation was supplied by an external cavity quantum cascade laser (QCL, Daylight Solutions) operating in the 6.92–7.57 μm (1320–1445 cm^{-1}) spectral region. The intrinsic linewidth of the laser is small enough (<10 MHz) to record Doppler-limited spectral lines. The frequency of the IR radiation was measured continuously by a spectrum analyzer (Bristol Instruments, model 771A-MIR), which had an accuracy of typically 1 ppm at the wavelengths considered here. Additional frequency calibration was performed using absorption measurements of calibration gases contained in an absorption cell; for details, see Appendix A. We estimate our final accuracy to be a few 0.001 cm^{-1} and the precision even better.

3. Results and analysis

The obtained laboratory spectrum of the ν_2/ν_4 bending vibrations of CH_3^+ is depicted in Fig. 1 and compared to a simulation obtained with the PGOPHER software (Western 2017). The lowest-lying ro-vibrational transitions, in particular those in the Q branch, are found to be readily saturated, unless very short laser interaction times of only a few tens of milliseconds are used. However, the overview spectrum displayed in Fig. 1 is recorded using a constant laser irradiation time of 840 ms to achieve a good spectral contrast for the highest lying rotational states. To visualize transition frequencies of these poorly populated quantum states, the simulated spectrum (lower trace in Fig. 1) was calculated at an elevated temperature of $T = 80$ K. A complete assigned linelist of the observed ro-vibrational transitions can be found in Appendix B. A combined spectroscopic fit of these 49 highly accurate lines and the high-resolution data of the ν_3 band reported by Jagod et al. (1994) yields spectroscopic constants, which are summarized in Table 1, and leads to well-defined band centers of 1405.8110(3) and 1395.2474(4) cm^{-1} for ν_2 and ν_4, respectively. A brief explanation of the spectroscopic constants and the details of the fit procedure can be found in Appendices C and D. Also in Table 1 is a comparison to the former parameters obtained by Changala et al. (2023). We note that those values were obtained by adjusting the initially ab initio computed spectroscopic parameters to the redshift-corrected JWST MIRI observations. MIRI with its resolution of 0.4 cm^{-1} permits to resolve single rovibrational lines potentially only in the P and R branches, whereas this is prohibited in the Q branch in a dense spectrum at 700 K. As a result of this congestion, a few assignments with high rotational excitation, J, of the former work are likely incorrect, for example the transition $(J, K, l) = (9, 1, -1) \leftarrow (10, 2, 0)$, and consequently some spectroscopic parameters in Table 1 differ, in particular the quartic distortion constants (D_J, D_{JK}, and D_K).

Table 1. Spectroscopic parameters of CH_3^+ in the ground vibrational state and the υ_2/υ_4 dyad.

Parameter	Changala *et al.* [a]	This work [b]
$\upsilon = 0$		
B	9.36123(15)	9.36175(10)
C	4.615768(49)	4.5942(14)
$D_J \times 10^3$	0.7263(17)	0.7344(10)
$D_{JK} \times 10^3$	−1.3072(25)	−1.310(2)
$D_K \times 10^3$	0.6296(44)	0.5276(9)
$H_J \times 10^9$	−0.189(63)	...
$\upsilon_2 = 1$		
ν_2	1405.743(58)	1405.8099(11)
B	9.3489(28)	9.3459(4)
C	4.6340(19)	4.630(9)
$D_J \times 10^3$	0.398(28)	0.73(3)
$D_{JK} \times 10^3$	−0.720(53)	−1.36(6)
$D_K \times 10^3$	0.375(33)	0.57(7)
$\upsilon_4 = 1$		
ν_4	1395.238(39)	1395.2471(15)
B	9.4488(22)	9.441(6)
C	4.57126(76)	4.557(4)
ζ_4	−0.10295(44)	−0.1114(3)
$\eta_{J,4} \times 10^3$	...	6.1(55)
$\eta_{K,4} \times 10^3$	...	−6.5(55)
$D_J \times 10^3$	0.809(24)	0.792(14)
$D_{JK} \times 10^3$	−1.370(46)	−1.44(4)
$D_K \times 10^3$	0.616(25)	0.59(3)
υ_2/υ_4		
F_{ab}	−8.9070(21)	−8.947(2)
$F_{ab,c}$	0.02232(20)	0.0227(9)
$F_{ab,J} \times 10^3$	...	1.73(3)
$F_{ab,K} \times 10^3$	...	−2.8(13)
Fit rms	0.064	0.0063

Notes. All values are in cm^{-1} (wavenumber) except that of ζ_4, which is dimensionless. Parameters for υ_3 are reported in Table D.1. [(a)]Values based on initially ab initio computed spectroscopic parameters, later refined by fitting to JWST MIRI data. See Changala et al. (2023) for details. [(b)]Global Fit of ν_2/ν_4 dyad and ν_3 data measured by Jagod et al. (1994). Errors on parameters (values in parentheses) are equal to 1σ.

4. Comparison to JWST data

Based on the spectroscopic constants of Table 1, with highly accurate band centers, a simulation of the CH_3^+ spectrum at a temperature of $T = 700$ K is presented in Fig. 2. It is compared with a new extraction of the astronomical emission of CH_3^+ in d203-506 from the same MIRI-MRS observations presented in Berné et al. (2023). We used a more recent version of the JWST Pipeline (version 11.17.14) which uses CRDS context file `jwst_1321.pmap`. This pipeline version claims to provide a wavelength calibration accuracy of ≈2 ± 2 km/s for point sources,

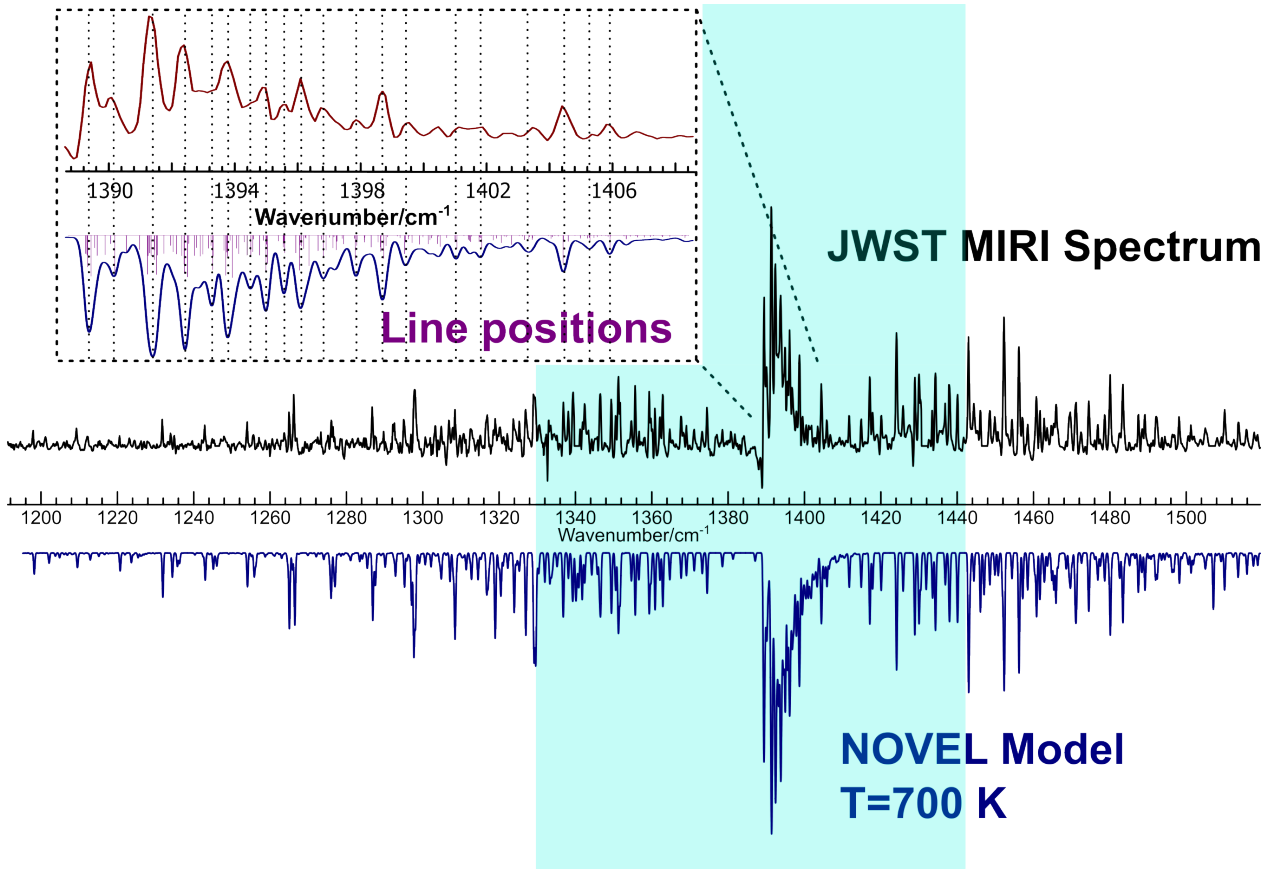

Fig. 2. Comparison of the 7 μm JWST MIRI spectrum of the disk d203-506 (*top*) with a simulation of CH_3^+ emission (*bottom*). The astronomical spectrum is a renewed extraction of the data presented in Berné et al. (2023), with the continuum and H_2 emission lines removed, but is otherwise not modified. The simulation is based on the accurate spectroscopic parameters given in Table 1 and calculated at a rotational temperature of T=700 K and FWHM=0.4 cm^{-1}. The zoom into the Q branch allows one to recognize a tiny shift in wavenumber between the calibrated laboratory data and the MIRI observation (see text for details). The shaded turquoise area marks the spectral range covered in the current laboratory measurements of Fig. 1.

which is improved by a factor of ∼10 with respect to the original spectrum. However, it is worth mentioning that for extended sources as in our case, there are systematic shifts of ≈5–10 km/s across the MIRI field of view. This systematic shift correction on extended sources is a current objective in the discs community but is of no major concern in our case, as the relative positions and intensities of emission lines are not affected by this shift. The excellent agreement between the accurate simulation and the JWST spectrum in Fig. 2 yields a final unequivocal confirmation of the recent astronomical detections of CH_3^+. A zoom into the Q branch (see the inset), reveals tiny frequency shifts with regard to the MIRI observation of the disk d203-506 in the Orion bar, in the range 0.02–0.06 cm^{-1}. This shift varies slightly from peak to peak and is difficult to specify, the reasons being that (i) the peaks are the convolution of several transitions (see stick spectrum in inset of Fig. 2), (ii) our model assumption of thermal equilibrium might not reflect the excitation conditions of CH_3^+ in d203-506, and (iii) the model's accuracy decreases at higher quantum numbers. A better calibrator is therefore, for example, the measured single line $J_K = 4_3 \leftarrow 3_3$ at 1424.1598 cm^{-1} (see Table B.1), which entirely dominates a strong peak in the MIRI spectrum, with a shift of 0.03 cm^{-1}. The radial velocities of known molecular tracers in the Orion bar are on the order of 10 km/s (Goicoechea et al. 2019), and more specifically the velocity of the disk d203-506 has been determined via HCO^+ observations to be 9.5 km/s (Champion et al. 2017), which corresponds to a wavenumber shift of 0.044 cm^{-1} at 7 μm. This is consistent with our above findings, within the above-stated calibration specification of MIRI of 2 ± 2 km/s (corresponding to 0.01 ± 0.01 cm^{-1}), and thus confirms the improvement of the MIRI calibration pipeline since the first CH_3^+ observation in 2023 (Berné et al. 2023; Changala et al. 2023).

5. Conclusions

With this work, all IR-active rovibrational fundamentals of CH_3^+ are finally characterized in high resolution, starting with the investigation of the ν_3 band in the 1980s (the ν_1 band is IR inactive). The high accuracy of the presented data for the ν_2/ν_4 Coriolis-coupled bands puts the JWST/MIRI data of ubiquitous CH_3^+ on a proper laboratory footing, allowing for confident quantum state assignments and the derivation of meaningful physical parameters such as temperature, density, and potentially source velocity. Similarly, the new data can serve as an accurate local wavenumber calibrator in the MIRI spectrum. These results may also stimulate renewed efforts toward the radio astronomical detection of deuterated versions of CH_3^+ (Roueff et al. 2013), the precise millimeter-wave transition frequencies of which are known from highly accurate laboratory measurements (Amano 2010; Töpfer et al. 2016; Jusko et al. 2017).

Looking back, 30 years ago the Oka group in Chicago was quite close to analyzing the ν_2/ν_4 band. In the thesis of Joo (1996), about 65 % out of the 95 lines measured in the 7 μm

region can now very likely be attributed to CH_3^+ (lines within 0.02 cm^{-1} of our simulation). A comparison of our simulation to their 370 K laser diode spectrum is given in Appendix E. Apparently, the patchy coverage of the diode lasers, interfering lines from other ionic species (e.g., CH_5^+), and the strong Coriolis coupling prevented a complete analysis at that time.

Finally, finding CH_3^+ as a potential key tracer of organic chemistry in space (Berné et al. 2023) calls for the search of other small hydrocarbon ions. High-resolution ro-vibrational and pure rotational spectra of the potential predecessor, CH_2^+, are becoming accessible with leak-out spectroscopy in the clean environment of a cryogenic ion trap. For the fully hydrogen saturated CH_5^+ first high-resolution IR spectra do exist (White et al. 1999; Asvany et al. 2015). Due to its floppiness, the spectrum is getting very complex, and its large partition function at any reasonable temperature is probably preventing its detection in the IR. Likewise, a rotational spectrum[1] is probably too weak because of a lacking dipole moment based on its high symmetry. Therefore, protonated methane might remain elusive in astronomical observations.

Data availability

The *xy*-trace of Fig. 1 and the PGOPHER file are available at https://zenodo.org/records/20743871 with DOI:https://doi.org/10.5281/zenodo.20743871.

Acknowledgements. This work has been supported by an ERC Advanced Grant (MissIons: 101020583), and by the Deutsche Forschungsgemeinschaft (DFG) via the Collaborative Research Centre SFB 1601 (project ID: 500700252, sub-project A6, B8, C3 and C4) and via SCHL 341/15-1 ("Cologne Center for Terahertz Spectroscopy"). P.B.C. was supported by NIST and the JILA PFC (NSF PHY-2317149).

References

Amano, T. 2010, A&A, 516, L4
Asvany, O., Padma Kumar P., Redlich, B., et al. 2005, Science, 309, 1219
Asvany, O., Bielau, F., Moratschke, D., Krause, J., & Schlemmer, S. 2010, Rev. Sci. Instr., 81, 076102
Asvany, O., Yamada, K. M. T., Brünken, S., Potapov, A., & Schlemmer, S. 2015, Science, 347, 1346
Asvany, O., Thorwirth, S., Redlich, B., & Schlemmer, S. 2018, J. Mol. Spectrosc., 347, 1
Asvany, O., Thorwirth, S., Schmid, P. C., Salomon, T., & Schlemmer, S. 2023, Phys. Chem. Chem. Phys., 25, 19740
Bast, M., Böing, J., Salomon, T., et al. 2023, J. Mol. Spectrosc., 398, 111840
Berné, O., Martin-Drumel, M.-A., Schroetter, I., et al. 2023, Nature, 621, 56
Bhatt, C., Cami, J., Peeters, E., et al. 2025, ApJ, 995, 67
Champion, J., Berné, O., Vicente, S., et al. 2017, A&A, 604, A69
Changala, P. B., Chen, N. L., Le, H. L., et al. 2023, A&A, 680, A19
Crofton, M. W., Kreiner, W. A., Jagod, M., Rehfuss, B. D., & Oka, T. 1985, J. Chem. Phys, 83, 3702
Crofton, M. W., Jagod, M., Rehfuss, B. D., Kreiner, W. A., & Oka, T. 1988, J. Chem. Phys., 88, 666
Cunha de Miranda, B. K., Alcaraz, C., Elhanine, M., et al. 2010, J. Phys. Chem. A, 114, 4818
Davies, P. B., & Smith, D. M. 1994, J. Chem. Phys., 100, 6166
Dopfer, O., & Luckhaus, D. 2002, J. Chem. Phys., 116, 1012
Goicoechea, J. R., Santa-Maria, M. G., Bron, E., et al. 2019, A&A, 622, A91
Gordon, I., Rothman, L., Hargreaves, R., et al. 2026, J. Quant. Spectrosc. Rad. Transf., 353, 109807
Gupta, D., Silva, W. G. D. P., Doménech, J. L., et al. 2023, Faraday Discuss., 245, 298
Gupta, D., Schmid, P. C., Salomon, T., Asvany, O., & Schlemmer, S. 2025, ACS Earth Space Chem., 9, 952
Henning, T., Kamp, I., Samland, M., et al. 2024, PASP, 136, 054302
Herbst, E., & Klemperer, W. 1973, ApJ, 185, 505
Jagod, M.-F., Gabrys, C. M., Rösslein, M., Uy, D., & Oka, T. 1994, Can. J. Phys., 72, 1192
Joo, S. 1996, PhD thesis, The University of Chicago, USA
Jusko, P., Stoffels, A., Thorwirth, S., et al. 2017, J. Mol. Spectrosc., 332, 59
Kawaguchi, K. 1994, Can. J. Phys., 72, 925
Keçeli, M., Shiozaki, T., Yagi, K., & Hirata, S. 2009, Mol. Phys., 107, 1283
Kraemer, W., & Špirko, V. 1991, J. Mol. Spectrosc., 149, 235
Meisner, J., Hallmen, P. P., Kästner, J., & Rauhut, G. 2019, J. Chem. Phys., 150, 084306
Nyman, G., & Yu, H.-G. 2019, AIP Adv., 9, 095017
Ragni, M., Bitencourt, A. C. P., Prudente, F. V., Barreto, P. R. P., & Posati, T. 2016, Eur. Phys. J. D, 70, 60
Rocha, W. R. M., McClure, M. K., Sturm, J. A., et al. 2025, A&A, 693, A288
Romero-Mirza, C. E., Öberg, K. I., Banzatti, A., et al. 2025, ApJ, 991, 128
Roueff, E., Gerin, M., Lis, D. C., et al. 2013, J. Phys. Chem. A, 117, 9959
Salomon, T., Baddeliyanage, C., Schladt, C., et al. 2025, Phys. Chem. Chem. Phys., 27, 4826
Schlemmer, S., Plaar, E., Gupta, D., et al. 2024, Mol. Phys., 122, e2241567
Schmid, P. C., Asvany, O., Salomon, T., Thorwirth, S., & Schlemmer, S. 2022, J. Phys. Chem. A, 126, 8111
Schmiedt, H., Schlemmer, S., & Jensen, P. 2015, J. Chem. Phys., 143, 154302
Silva, W. G. D. P., Cernicharo, J., Schlemmer, S., et al. 2023, A&A, 676, L1
Silva, W. G. D. P., Bonah, L., Schmid, P. C., Schlemmer, S., & Asvany, O. 2024a, J. Chem. Phys., 160, 071101
Silva, W. G. D. P., Gupta, D., Plaar, E., et al. 2024b, Mol. Phys., 122, e2296613
Steenbakkers, K., van Boxtel, T., Groenenboom, G. C., et al. 2024, Phys. Chem. Chem. Phys., 26, 2692
Thomas, R. D., Kashperka, I., Vigren, E., et al. 2012, ApJ, 758, 55
Töpfer, M., Jusko, P., Schlemmer, S., & Asvany, O. 2016, A&A, 593, L11
Western, C. M. 2017, J. Quant. Spectrosc. Rad. Transf., 186, 221
White, E. T., Tang, J., & Oka, T. 1999, Science, 284, 135
Yu, H.-G., & Sears, T. J. 2002, J. Chem. Phys., 117, 666
Zannese, M., Tabone, B., Habart, E., et al. 2025, A&A, 696, A99

[1] Strictly speaking CH_5^+ does not exhibit a pure rotational spectrum by symmetry considerations; see Schmiedt et al. (2015).

Appendix A: Laboratory calibration procedure

The frequency of the IR radiation has been continuously measured by a wavemeter. In order to check and potentially improve the accuracy of these measurements, an additional calibration using a 15 cm long reference gas cell has been applied. The cell was originally filled with 20 mbar of pure N_2O. A linewidth analysis of the determined N_2O reference gas lines yielded an actual nominal pressure of 161 mbar inside the cell, the increased pressure being attributed to leaking-in ambient air. Therefore, also one water line (water contained in the air of the cell) could be used as calibrator. The difference between the nominal ν_{nom} and measured ν_{obs} transition frequencies yielded the calibration of the spectrum, with the nominal transition frequencies ν_{nom} determined by taking into account the pressure shift at a pressure of 161 mbar inside the cell. The outcome of the individual calibration measurements is listed in the table below. An average offset of -0.0009 cm^{-1} of the wavemeter readout is observed, which is well within the manufacturer's stated absolute accuracy of 1 ppm. Reference line positions as well as pressure shift coefficients are taken from the HITRAN database (Gordon et al. 2026).

Table A.1. Observed calibration lines.

$\nu_{obs.}$ / cm^{-1}	ν_{Hitran} / cm^{-1}	δ_{Air} / $cm^{-1}atm^{-1}$	$\nu_{obs.} - \nu_{nom}$ / cm^{-1}
1333.3925	1333.3938	-0.0014	-0.0010
1333.5760	1333.5762	-0.0013	0.0002
1333.5899	1333.5919	-0.0013	-0.0018
1333.5205	1333.5215	-0.0015	-0.0007
1333.5299	1333.5305	-0.0014	-0.0003
1333.3933	1333.3938	-0.0014	-0.0004
1333.5206	1333.5215	-0.0015	-0.0006
1333.5295	1333.5305	-0.0014	-0.0007
1330.1319	1330.1335	-0.0013	-0.0015
1330.1320	1330.1335	-0.0013	-0.0014
1330.1240	1330.1253	-0.0013	-0.0011
1330.1245	1330.1253	-0.0013	-0.0005
1330.0599	1330.0608	-0.0014	-0.0007
1330.0598	1330.0608	-0.0014	-0.0008
1330.5086	1330.5095	-0.0015	-0.0007
1329.6411	1329.6426	-0.0014	-0.0013
1329.6409	1329.6426	-0.0014	-0.0015
1329.6405	1329.6426	-0.0014	-0.0018
1340.1665	1340.1667	0.0039	-0.0009

Notes. Observed transitions of N_2O at a nominal pressure of 161 mbar compared to the vacuum transition wavenumbers listed in the HITRAN database (Gordon et al. 2026). The nominal transition frequencies ν_{nom} have been calculated using the given pressure shift coefficients δ_{Air}. All reference lines are N_2O except the one separated by a horizontal line, which is from H_2O. The line profile of the H_2O line has two contributions arising from water vapour in laboratory air (broad Lorentzian) and water vapour in the reference gas cell (sharp Lorentzian). Its center frequency is given with respect to the sharp lower pressure component.

Appendix B: Transition frequencies

The line center frequencies are given in Table B.1.

Appendix C: Spectroscopy of CH_3^+

The molecule CH_3^+ is a planar symmetric top belonging to the D_{3h} group of symmetry. It possesses four fundamental vibrational modes, ν_1 through ν_4, of which the last two, ν_3 and ν_4, are doubly degenerate. The rotational energy levels are classified by two quantum numbers, the total angular momentum quantum number J, and its projection onto the symmetry axis, K. An additional vibrational angular momentum quantum number, $l = \pm 1$, is needed for the description of the states ν_3 and ν_4, and accounts for first-order Coriolis-coupling in those

Table B.1. Observed transitions of the ν_2/ν_4 bending vibration of CH_3^+ (in cm^{-1}).

	J'	K'	l^a	J''	K''	obs / cm^{-1}
ν_4	5	5	-1	6	6	1329.6285
ν_2	2	2		3	2	1333.4349
ν_4	4	4	-1	5	5	1340.1263
ν_4	4	3	-1	5	4	1349.4092
ν_4	3	3	-1	4	4	1350.5411
ν_2	1	1		2	1	1352.6374
ν_4	4	2	-1	5	3	1355.6816
ν_4	3	2	-1	4	3	1359.3436
ν_4	2	2	-1	3	3	1360.8765
ν_4	3	1	-1	4	2	1364.7276
ν_4	3	0	±1	4	1	1367.7013
ν_4	2	1	-1	3	2	1369.0859
ν_4	1	1	-1	2	2	1371.1270
ν_4	2	0	±1	3	1	1373.2306
ν_4	2	1	1	3	0	1374.5166
ν_4	1	0	±1	2	1	1378.5051
ν_4	0	0	±1	1	1	1381.2923
ν_2	0	0		1	0	1387.0896
ν_2	4	4		4	4	1389.2755
ν_2	5	5		5	5	1389.3193
ν_2	3	3		3	3	1389.3385
ν_2	6	6		6	6	1389.4431
ν_2	2	2		2	2	1389.5589
ν_2	1	1		1	1	1390.0671
ν_4	4	4	1	4	3	1391.2350
ν_4	5	5	1	5	4	1391.2535
ν_4	3	3	1	3	2	1391.3024
ν_4	2	2	1	2	1	1391.4577
ν_4	1	1	1	1	0	1391.5431
ν_4	3	2	1	3	1	1392.1531
ν_4	4	3	1	4	2	1392.3216
ν_4	3	1	1	3	0	1392.4061
ν_4	5	4	1	5	3	1392.5043
ν_4	4	2	1	4	1	1392.9024
ν_2	2	0		1	0	1404.4211
ν_2	2	1		1	1	1405.9090
ν_2	3	1		2	1	1411.7342
ν_2	3	2		2	2	1414.8703
ν_2	4	0		3	0	1417.1291
ν_2	4	1		3	1	1417.8512
ν_2	4	2		3	2	1420.0970
ν_2	4	3		3	3	1424.1598
ν_2	5	2		4	2	1425.8584
ν_4	2	2	1	1	1	1428.8886
ν_2	5	3		4	3	1428.9134
ν_2	5	4		4	4	1433.5609
ν_2	6	3		5	3	1434.3283
ν_2	6	4		5	4	1437.9371
ν_2	6	5		5	5	1442.9758

Notes. The line frequencies were measured with a wavemeter and calibrated following the procedure described in Appendix A. The accuracy of the lines is a few 0.001 cm^{-1} (wavenumber) and the precision better than 0.001 cm^{-1}. $^{(a)}$values for ℓ are given for transitions associated with the unperturbed ν_4 vibrational mode. For K=0 the two l-components collapse.

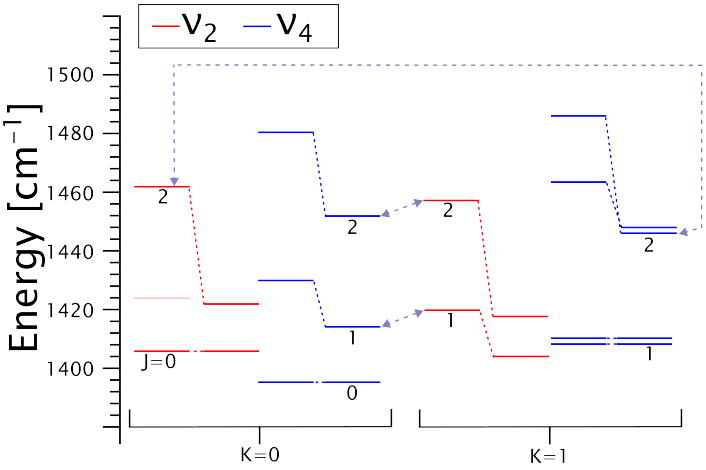

Fig. C.1. Energy term diagram of the Coriolis coupled ν_2/ν_4 dyad for the rotational states up to J=2, K=1. Unperturbed ($F_{ab} = F_{ab,c} = F_{ab,J} = F_{ab,K} = 0$) and perturbed energy terms are drawn as horizontal solid lines with the J rotational quantum number displayed only for the unperturbed level. States subject to Coriolis interaction are connected by grey dashed arrows. Slanted dashed colored lines connecting energy levels show the energy shifts resulting from the Coriolis interaction.

degenerate states. As an additional complication, owing to the accidental near-degeneracy and strong Coriolis interactions between ν_2 and ν_4, their zeroth-order K and ℓ quantum numbers are highly mixed in their rotational manifolds.

In Fig. C.1 we show an energy term diagram of the two vibrational modes ν_2 (red levels) and ν_4 (blue levels) for selected rotational states in order to illustrate the influence of the Coriolis interaction between them because this made the spectroscopic analysis challenging from the start. The energy terms for the unperturbed system ($F_{ab} = F_{ab,c} = F_{ab,J} = F_{ab,K} = 0$ with all remaining parameters equivalent to values given in Table 1) are those which are labeled by the appropriate (J,K) rotational quantum numbers. Within this model of unperturbed vibrational modes, the energy levels in a given vibrational state are calculated using the two rotational constants ($A = B$ and C), centrifugal distortion parameters (D_J, D_{JK}, D_K...), and, for the degenerate states ν_3 and ν_4, additional Coriolis-coupling and ℓ-type doubling parameters (ζ, η_J, q).

Colored dashed lines in Fig. C.1 connect these unperturbed energy terms with those of the perturbed system, indicating how these levels are shifted by the Coriolis interaction between the vibrational modes ν_2 and ν_4. This second set of terms marks the energies reconstructed from fitting the complete spectroscopic model to the measured transition frequencies. Closer inspection of Fig. C.1 reveals that for J=2 and K=0 of the ν_2 mode the level is shifted about -40 cm^{-1} which puts this level even below the unperturbed J=1 level. A grey dashed arrow links the unperturbed state to the corresponding interacting (2, 1) state of ν_4. This level is pushed up by a similarly large value. In fact, this (2, 1) level consists of two levels belonging to the two $\ell = \pm 1$ values associated with the vibrational angular momentum of this degenerate molecular vibration. These states which are only showing a small ℓ-type doubling in the unperturbed situation are exhibiting a large splitting due to the Coriolis interaction as seen in the diagram. Two more examples of coupling states are indicated by more dashed arrows linking two more close lying states. It is interesting to see how the few additional ν_2/ν_4 spectroscopic parameters F_{ab}, $F_{ab,c}$, $F_{ab,J}$, and $F_{ab,K}$ listed in Table 1 account very well for the quite large Coriolis interaction in CH_3^+ which often couples a number of states as K and ℓ are no longer good quantum numbers of the system, yet, we use them to assign the levels in Table B.1 in a unique way.

Appendix D: Fit details

Similar to the procedure presented in the previous work by Changala et al. (2023), the spectroscopic constants reported here are derived from a combined fit of both the ν_2/ν_4 dyad from this work and the ν_3 band from Jagod et al. (1994). The inclusion of the ν_3 band helps to better constrain the molecular parameters (see also below). The data of Joo (1996) were not included. The measurements from Jagod et al. (1994) were weighted according to their expected experimental accuracy, that is, 0.0035 cm^{-1}, while those observed in this work are weighted according to the root-mean square of the ν_2/ν_4 dyad, that is, 0.0007 cm^{-1}. The best-fit parameters of the $v = 0$, $v_2 = 1$ and $v_4 = 1$ states are reported in Table 1 while those of $v_3 = 1$ are reported here in Table D.1. The root-mean square errors of the lower state combination differences are 0.0045 cm^{-1} for the ν_3 band and 0.001 cm^{-1} for the ν_2/ν_4 dyad, proving the stated experimental accuracies. Meanwhile, excited state combination differences are 0.0093 cm^{-1} for the ν_3 band and 0.0007 cm^{-1} for the ν_2/ν_4 dyad. The slightly worse excited state root-mean square error of the ν_3 band is attributed to the variety of local perturbations reported by Jagod et al. (1994). The fit residuals are depicted in Fig. D.1. We note that 46 of the 49 transitions reported for the ν_2/ν_4 dyad in Table B.1 obey the restrictive quasi-spherical-top selection rules ($\Delta|k - \ell| = 0$, $\Delta\tau = \Delta J$) discussed by Changala et al. (2023). Only the P(3) transition at 1333.4349 cm^{-1}, the P(2) transition at 1352.6374 cm^{-1}, and the R(1) transition at 1428.8886 cm^{-1} violate these rules owing to imperfect destructive interference between the ν_2 and ν_4 transition dipole matrix elements (0.060 D and 0.073 D, respectively).

The C rotational constants are affected by the Coriolis coupling constants. Fortunately, the high degree of symmetry of CH_3^+ leads to extensive sum rules constraining the values of the Coriolis parameters. From these relations, we can infer that the expected values of the lowest-order Coriolis parameters, ζ_4 and ζ_3, are similar in magnitude but opposite in sign (see Changala et al. 2023; Crofton et al. 1988):

$$\zeta_4 \approx -\zeta_3 \ .$$

A combined fit of both the ν_2/ν_4 dyad and the ν_3 fundamental is therefore performed in which the above correlation is strictly enforced. The results of this fit are listed in Tables 1 and D.1. The PGOPHER file is available as `supplementary material`.

Appendix E: Comparison to former measurement

In the thesis of Joo (1996), 95 lines were attributed to the bending vibration of CH_3^+, albeit without giving any quantum number assignment. The lines have an estimated accuracy of 0.005 cm^{-1}, and the temperature of the cooled discharge was estimated to be around 370 K. In Fig. E.1 these 95 lines are compared to a simulation based on our constants given in Table1. Although the agreement seems quite suggestive, in particular in the Q branch, the differences between our model and the lines from Joo (1996) are on the order of 0.02 cm^{-1}, and very often even larger. It is thus difficult to distinguish between a CH_3^+ line with limited accuracy and a contaminating line, for example those of CH_5^+ (see Fig. 2A of Asvany et al. 2005). For this reason, the data of Joo (1996) were not included in our analysis.

Table D.1. Spectroscopic constants of CH_3^+ in the v_3 band.

Parameter	Changala et al. (2023)[a]	This work[a]
ν_3	3108.3804(14)	3108.3547(20)
B	9.27152(15)	9.27239(11)
C	4.574692(36)	4.5537(14)
ζ_3	0.115685(49)	0.1114(3)
$D_J \times 10^3$	0.6922(15)	0.7040(11)
$D_{JK} \times 10^3$	−1.2882(26)	−1.298(3)
$D_K \times 10^3$	0.6405(45)	0.5406(8)
$H_J \times 10^9$	−0.146(49)	
$q \times 10^3$	7.15(20)	9.5(2)
$\eta_J \times 10^3$	−0.638(10)	−0.671(9)
$\eta_K \times 10^3$	0.682(19)	0.311(9)
$Dq_J \times 10^3$	0.0266(22)	0.035(3)
$Dq_K \times 10^3$	0.665(21)	−0.71(2)

Notes. All values are in cm^{-1} except that of ζ_3, which is dimensionless.
[(a)]Errors on parameters (values in parentheses) are equal to 1σ.

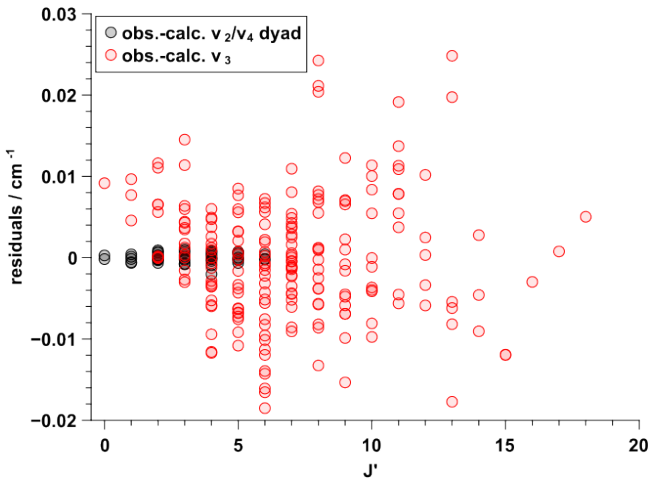

Fig. D.1. Residuals (in cm^{-1}) of the novel line-by-line fit plotted as a function of the excited state rotational quantum number. The large residuals for ν_3 are caused by perturbations (Crofton et al. 1988; Jagod et al. 1994).

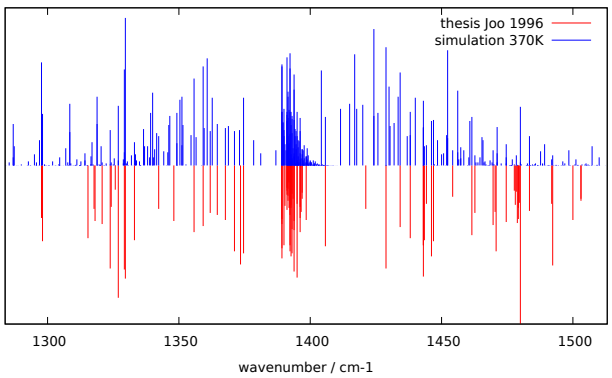

Fig. E.1. Comparison of a 370 K simulation of the bending motion of CH_3^+ with the results obtained by Joo (1996).